ARTICLE OPEN

Check for updates

Psychedelic neuroplasticity of cortical neurons lacking 5-HT2A receptors

Tyler G. Ekins[1,2,6], Chloe Rybicki-Kler[1,3,6], Tao Deng[1], Isla A. W. Brooks[1], Izabela Jedrasiak-Cape[1], Ethan Donoho[1] and Omar J. Ahmed[1,2,3,4,5]✉

© The Author(s) 2025

Classical psychedelic drugs show promise as a treatment for major depressive disorder and related psychiatric disorders. This therapeutic efficacy stems from long-lasting psychedelic-induced neuroplasticity onto prefrontal cortical neurons and is thought to require the postsynaptic expression of serotonin 2A receptors (5-HT_{2A}R). However, other cortical regions such as the granular retrosplenial cortex (RSG) – important for memory, spatial orientation, fear extinction, and imagining oneself in the future, but impaired in Alzheimer's disease – lack 5-HT_{2A}R and are thus considered unlikely to benefit from psychedelic therapy. Here, we show that RSG pyramidal cells lacking postsynaptic 5-HT_{2A} receptors still undergo long-lasting psychedelic-induced synaptic enhancement. A newly engineered CRISPR-Cas-based conditional knockout mouse line reveals that this form of psychedelic-induced retrosplenial plasticity requires presynaptic 5-HT_{2A} receptors expressed on anterior thalamic axonal inputs to RSG. These results highlight a broader psychedelic therapeutic utility than currently appreciated, suggesting potential for augmenting RSG circuit function in Alzheimer's disease, post-traumatic stress disorder, and other neuropsychiatric conditions, despite the lack of postsynaptic 5-HT_{2A} receptors.

Molecular Psychiatry (2026) 31:1431–1442; https://doi.org/10.1038/s41380-025-03257-w

INTRODUCTION

Classical serotonergic psychedelic drugs induce powerful perceptual experiences and show increasing promise for the treatment of a range of neuropsychiatric disorders [1–13]. Classical psychedelic drugs share a common affinity for serotonin 2A (5-HT_{2A}) receptors [14–22]. Signaling cascades induced by activation of 5-HT_{2A} receptors result in a lasting enhancement of synaptic connections in the prefrontal cortex (PFC), and this synaptogenic effect is thought to provide a main neurobiological basis underlying psychedelic medicine [23–30]. Direct expression of 5-HT_{2A} receptors on the postsynaptic neuron, encoded by the gene *Htr2a*, is thus considered necessary for psychedelic-induced dendritic spine formation in the prefrontal cortex [11–13, 21–30].

Many pyramidal cells in cortex do not, however, express 5-HT_{2A} receptors [31–38]. As postsynaptic activation of 5-HT_{2A} receptors is considered essential for psychedelic-induced neuroplasticity, the prevailing assumption is that psychedelics would not offer therapeutic benefit in cells and regions that directly lack 5-HT_{2A} receptors [21–30]. Psychedelic medicine therefore has primarily focused on treating disorders traditionally associated with prefrontal and cingulate cortex where 5-HT_{2A} receptors are strongly expressed, including major depressive disorder and PTSD [11–13, 39–41].

The granular retrosplenial cortex (RSG) is perhaps the starkest example of a cortical region lacking pyramidal cell 5-HT_{2A} receptors. The RSG is part of the default mode network, integrating synaptic inputs from thalamic, cortical, hippocampal, and claustral sources to support functions ranging from memory, spatial orientation, and imagining oneself in the future [42–55]. In humans, damage to the retrosplenial cortex produces memory impairments and spatial disorientation, resulting in a dramatic inability to even find one's way home [56–60]. The RSG is also one of the first regions to show hypoactivity in the earliest stages of Alzheimer's disease, with almost all people living with advanced Alzheimer's disease going on to experience severe spatial disorientation symptoms associated with RSG dysfunction [57, 58, 61]. The RSG also plays a critical role in the appropriate processing of fear, as well as the successful extinction of fearful memories [46, 55]. It is not known if classical psychedelics can boost synaptic activity and induce spinogenesis in 5-HT_{2A} receptor-lacking RSG principal neurons. The answer to this question is of critical importance, as it would open the possibility of using psychedelics to correct RSG-specific synaptic deficits in Alzheimer's disease & fear-related disorders, as well as motivate attempts to treat other disorders involving neurons not directly expressing 5-HT_{2A} receptors.

Here, using genetic engineering of a new 5-HT_{2A} receptor (*Htr2a*) conditional knockout (cKO) mouse line, ex vivo intracellular physiology, pharmacology, optogenetics, cellular morphology, and single-nucleus/spatial transcriptomics, we test the hypothesis

[1]Dept. of Psychology, University of Michigan, Ann Arbor, MI 48109, USA. [2]Michigan Psychedelic Center, University of Michigan, Ann Arbor, MI 48109, USA. [3]Neuroscience Graduate Program, University of Michigan, Ann Arbor, MI 48109, USA. [4]Dept. of Biomedical Engineering, University of Michigan, Ann Arbor, MI 48109, USA. [5]Center for Computational Medicine & Bioinformatics, University of Michigan, Ann Arbor, MI 48109, USA. [6]These authors contributed equally: Tyler G. Ekins, Chloe Rybicki-Kler.
✉email: ojahmed@umich.edu

Received: 16 November 2024 Revised: 12 August 2025 Accepted: 5 September 2025
Published online: 16 September 2025

that psychedelics can increase synaptic connections of RSG neurons lacking 5-HT_{2A} receptors. The *Htr2a* cKO line allows for the synapse-specific dissection of rules governing psychedelic-induced strengthening of synaptic connectivity and reveals a presynaptic, but not postsynaptic, requirement for 5-HT_{2A} receptors to boost retrosplenial synaptic activity and dendritic spines. This work expands the catalog of neurological and psychiatric disorders that psychedelic medicine may be able to potentially treat via lasting synaptic enhancement.

METHODS

Animals

All procedures and use of animals were approved by the University of Michigan Institutional Animal Care and Use Committee. Mouse lines were obtained from Jackson Laboratories unless specified. The following mouse lines were used for whole cell recordings: Ai14, Ai32, C57BL/6J, Cux2-Cre, Grp-Cre, *Htr2a*-floxed (*Htr2a*^{fl}), Kj319. Nex-Cre, Pvalb-Ai14, Pvalb-Cre, Scnn1a-Cre, Syt6-Cre. All mice used in the experiments were bred on a C57BL6 background (Charles River). A combined total of 321 neurons from 84 mice of both sexes between the ages of postnatal days 30–306 were used.

Creation and validation of *Htr2a* conditional knockout mice

With the University of Michigan Transgenic Animal Model Core, we utilized the CRISPR-Cas9 system in C57BL/6 mouse embryos to introduce two LoxP sites flanking the *Htr2a* Exon 1 protein-coding region (*Htr2a*^{fl}). Single-stranded RNA guides (Supplementary Table 1) were complexed with Integrated Data Technologies HiFi Cas9 protein (IDT # 1081060) before co-injection with donor DNA into embryos. HiFi Cas9 protein is designed for high specificity of on-target activity [62]. To validate that the LoxP insertions were successful, we performed PCR genotyping using the primers specified in Supplementary Table 1. G0 founders were bred with wild-type mates to create heterozygous G1 mice, which we bred in-house to homozygosity (*Htr2a*$^{fl/fl}$) before use in experiments.

RNAScope

RNAScope was used to confirm presence of *Htr2a* mRNA in prefrontal cortex (PFC) and anterior dorsal (AD) thalamus. RNAScope was also used to validate loss of *Htr2a* mRNA after viral transfection of Cre. We used three *Htr2a*$^{fl/fl}$ mice injected with AAV2-Cre-eGFP into PFC (P93-162) as described in the Surgical Procedures. The virus was allowed to incubate for at least 4 weeks before the start of the RNAScope assay. Two of the three animals were deeply anesthetized with isoflurane, perfused, and the brain dissected into 10% neutral buffered formalin (Sigma #HT501128) for overnight fixation. Next day the brain was moved to 70% ethanol and used for paraffin embedding and subsequent RNAScope. One animal was deeply anesthetized with Isoflurane, decapitated, and the brain was dissected and immediately snap-frozen on dry ice and kept at −80 °C until the start of the experiment (7 days). Then, the brain was sliced on a cryostat (Leica 3050S) at 14 µm and mounted onto charged slides (Fisher Scientific #12-550-15). Mounted slices were kept overnight at −80 °C degrees and used next day for RNAScope.

Immediately prior to starting the assay, frozen slides were placed in 10% neutral buffered formalin for 1 h fixation at 4 °C, then dehydrated in series ethanol steps (50, 70, and 100%). Afterwards, a barrier was drawn around each slice using a hydrophobic pen (ACD # 310018), and all the subsequent reagents used were part of the RNAScope® Multiplex Fluorescent Reagent Kit v2 (ACD #323100) unless indicated otherwise. Endogenous peroxidase activity was then blocked with hydrogen peroxide solution, and the tissue permeabilized with protease IV.

After pretreatment, a custom *Htr2a* probe was prepared (ACD). The custom *Htr2a* probe was designed to target the floxed sequence of the *Htr2a* gene in the *Htr2a*$^{fl/fl}$ mouse line. The probe was applied to slices, allowed to hybridize for 2 h at 40 °C and was then washed off using the wash buffer. The probe were then amplified using a series of three amplification steps, and fluorescent signal was developed using TSA Vivid 650 (ACD #323273). The signal development round was carried out at 40° C and consisted of the channel-specific HRP incubation, fluorescent dye application, and HRP blocking, with wash buffer washes after each step. Finally, the slices were mounted with FluoromountG with DAPI (Southern Biotech #0100-20), cover slipped, and set overnight at 4 °C. Confocal imaging was then carried out.

Pharmacology

25CN-NBOH was purchased from Tocris Bioscience and was administered to mice via intraperitoneal (IP) injection (2, 10, or 20 mg/kg, specified throughout text), dissolved in sterile saline, brought up to a volume equaling no more than 1% of the mouse's total bodyweight. Brief sonication was used to aid solubility. Mice were moved to single housing before injection and recorded 24–72 h post-injection. For acute pharmacology recordings, 25CN-NBOH (final concentration = 10 µM) was diluted into artificial cerebral spinal fluid (ACSF) from a stock concentration dissolved in sterile water.

Surgical procedures

Surgical anesthesia was induced via vaporized isoflurane inhalation at 5% and then maintained at 1–3% isoflurane. Upon induction, atropine was injected subcutaneously at 0.05 mg/kg. A Physitemp (Clifton, New Jersey, USA) controller monitored and maintained body temperature at 37 °C. Ophthalmic ointment was placed on the eyes. The incision site was prepared using a wash of Nolvasan (1:40) followed by isopropyl alcohol and then a subcutaneous injection of lidocaine (1%). The skull was cleaned using Hydrogen Peroxide, then leveled using bregma and lambda. Using a digital stereotaxic coordinate system, the following injection target sites were identified: right anterodorsal (AD) thalamic nucleus for ChR2 experiments (AP = −0.6 mm, ML = ± 0.78 mm, DV = −2.5, −3.25 mm), and both AD thalamic nuclei for Cre-GFP injection. Craniectomies were performed at the target sites, and then dura at the target coordinates was removed. Micropipettes were lowered under stereotaxic guidance into the target injection site containing the ChR2 viral construct (AAV2-EF1a-DIO-hChR2(h134R)-eYFP or Cre/GFP viral construct (AAV2-hSyn-GFP-Cre), obtained from UNC Gene Therapy Vector Core. Injections of 2.0 µL total virus volume were administered via a picospritzer (0.05–0.07 µL/min). After injection, there was a 10-min period before removing the micropipette from the brain. Enrofloxacin was administered (8.0 mg/kg) after injections. Craniectomies were sealed with bone wax, the skin incision was closed with VetBond, and with antibiotic ointment placed under skin edges. Isoflurane was tapered down prior to removal, after which carprofen was administered (5 mg/kg). Mice were kept warm through an artificial heat source during the recovery period. Mice then recovered for 3–6 weeks post-injection before being used in experiments.

Slice preparation

Brains were dissected in ice-cold sucrose-substituted ACSF, saturated with 95% O2 and 5% CO2 and containing the following (in mM): 3 KCl, 1.25 NaH2PO4, 26 NaHCO3, 10 dextrose, 234 sucrose, 0.2 CaCl2, 4 MgSO4. 300 µm coronal slices were cut using a Leica Microsystems 1200VT vibratome and placed in a high-magnesium ACSF solution at 32 °C for 30 min and subsequently rested at room temperature for at least 30 more minutes before being recorded. During experiments, slices were submerged in a recording chamber with physiological temperature (32 °C) ACSF (126 mM NaCl, 1.25 mM NaH2PO4, 26 mM NaHCO3, 3 mM KCl, 10 mM dextrose, 1.20 mM CaCl2, and 1 mM MgSO4) perfused at 3 mL/min. Slices containing retrosplenial cortex (RSC) were obtained from anteroposterior (AP) distance to bregma −1.0 to −3.7 mm; slices containing anterior cingulate cortex (ACC) were obtained from AP 2.1 to −0.5 mm; slices containing anterodorsal thalamus (AD) were obtained from AP −0.4 to −0.9 mm.

Whole-cell electrophysiology and quality control

Neurons were visualized on an Olympus BX51WI microscope, Olympus 60× water immersion lens, and Andor Neo sCMOS camera (Oxford Instruments, Abingdon, Oxfordshire, UK). Patch electrodes were pulled from borosilicate glass (Sutter Instruments; diameter 1.5 × 0.86 mm) to a tip resistance between 4–6 MΩ. The internal solution was potassium gluconate-based and contained (in mM): 130 K-gluconate, 0.6 EGTA, 10 HEPES, 2 MgATP, 0.3 Na2GTP, 6 KCl, NaCl and 0.5% biocytin (calculated $E_{Cl} = -68$ mV; pH = 7.25; osmolarity = 290 mOsm). Pipette capacitance compensation and bridge balance were applied; recordings were not corrected post-hoc for liquid junction potential. In ACC, only L5 neurons with regular spiking firing patterns that did not fire rebound spikes after hyperpolarizing current injection were used in this study. In RSG, LR cells in L2/3 were identified by characteristic firing patterns as previously described [48, 49, 53]. Cells were excluded if baseline resting membrane potential was more depolarized than −55 mV (or −45 mV for AD thalamus recordings), if input resistance decreased >25% before acute pharmacology experiments, if uncompensated series resistance (Rs) was >35 MΩ, or if

Δ Rs >25% during acute pharmacology experiments. All whole-cell recordings were conducted with MultiClamp 700B amplifier and digitized at 20 kHz with Digidata 1550B (Molecular Devices) for collection on a computer equipped with pClamp 10.7 software (Molecular Devices). Patch electrodes additionally contained biocytin (0.5%), which enabled post-hoc imaging (see methods below) to determine somatic position and confirm cellular morphology. In ACC, we considered L5 neurons to have cell bodies 125 to 400 microns from the L1/2 border. In RSG, L2/3 was identified visually by the densely packed granular cell layer.

Cell filling and imaging

Internal solutions for all recorded neurons contained biocytin to enable post-hoc morphological analysis [29, 48, 49, 63, 64]. Cells were recorded for at least 15 min to allow diffusion of biocytin throughout the neuron. Upon completion of recording, the pipette was carefully retracted to enable membrane resealing and the slice was immediately transferred to 4% PFA for overnight fixation. After fixation, slices were washed in phosphate buffer solution (PBS) three times (ten minutes) and incubated in PBS containing 0.4% triton, fluorescent nissl (NeuroTrace 435/455), and 1:1000 streptavidin conjugated Alexa Fluor 647 at 4 °C (48 h). Afterwards, slices were washed in PBS, mounted with FluoromountG and allowed to rest for at least 24 h before imaging. Imaging was conducted with a Zeiss Axio Image M2 microscope equipped with LSM 700 confocal system using a 63× oil objective lens as z-stacks with z-step of 0.4 µm. Neurons were then reconstructed from these files using NeuTube 1.0 software.

Spine classification and density analysis

Spines were analyzed by an experimenter blinded to experimental conditions. For each neuron imaged, a representative main apical dendrite as well as apical tuft dendrites we imaged using a Zeiss Airyscan system. Dendrite lengths were measured in FIJI ImageJ. Spine counts were tracked using the Cell Counter plugin in FIJI. Cells that filled uniformly and had no major cut off branches were selected for further spine analysis. Z-stacks of the dendrites were obtained using a Zeiss Airyscan confocal microscope system. The z-stacks were processed in ImageJ, and the spines manually identified and counted with the "cell counter" plugin based on visual inspection. Spines are defined by visibly clear protrusions on dendrites. Up to 5 apical dendrites and up to 5 basal dendrites were selected for each neuron, and each dendrite was independently analyzed. To enable a reliable spine density measurement, branches shorter than 40 microns were not included. Note that LR neurons have fewer, thinner, and smaller dendritic branches than RS cells. The spine density for each dendrite was calculated as the number of spines on the segment divided by the length of the dendrite. For spine reconstructions, max projections of Z-stacks were obtained from the high resolution 3-D images for each group, and 5 um scale bars are added to the images with the 'Scale Bar' tool from ImageJ. One representative dendrite was then selected from each group and manually traced with Procreate.

Analysis of spontaneous synaptic activity

Voltage-clamp recordings were conducted at a holding potential of −70 mV. sEPSC recordings were taken in 30-second sweeps with a brief (250 ms) hyperpolarizing test pulse (−5 mV) at the start to monitor Rs and Rin throughout the experiment. Spontaneous excitatory post-synaptic currents (sEPSCs) were analyzed by an experimenter blinded to experimental conditions using Easy Electrophysiology (version 2.4.0) in 29-second sweeps (the first second of each sweep contained the test pulse and was thus discarded). Putative events were identified with threshold-based detection (negative peak direction, 5 ms local maximum period, 30 ms decay search period, 8 pA threshold, 10 ms search period, 1-ms averaged baseline, curved baseline and threshold). Events were manually inspected, and noise events were rejected to eliminate false positive events. Frequency was determined for each sweep by diving the total number of events per sweep by 29 s, amplitude was computed by averaging all events for each sweep, half-width and decay time constant were determined from fitting an exponential to the averaged event for each sweep. During acute pharmacology experiments, sEPSCs are recorded for two consecutive sweeps in standard ACSF, immediately before switching to the drug-containing ACSF and recording sEPSCs for 20 more sweeps. In some cases, optogenetic stimulation (described below) was additionally used during acute pharmacology experiments. Stimulation occurred after the test pulse, and thus the first 2 s of every sweep were discarded for sEPSC analysis.

Analysis of optogenetic-evoked synaptic activity

Optogenetic brain slice experiments were conducted on the same rig set-up using a 5500 K white light-emitting diode (LED; Mightex; maximum power of 14.47 mW measured at the slice focal plane). Synaptic responses to optical stimulation of the ChR2-expressing thalamic axons were measured from postsynaptic retrosplenial neurons recorded under whole-cell current-clamp or voltage-clamp conditions while optically stimulating L3. Synaptic responses were obtained from 10 Hz stimulation (10 pulses, 1 ms pulse-width, 4–5 trials). During voltage-clamp pharmacology experiments, after establishing a baseline response (1 ms pulse-width, 30 s sweeps), 25CN-NBOH was bath-applied for 10 min and RMP and evoked EPSC amplitude continued to be recorded under identical stimulation parameters. After the 10-min perfusion, the 10 Hz voltage clamp synaptic responses were again recorded (10 pulses, 1 ms pulse-width, 5 trials). The amplitude of the first pulse (pA), and the area (pA*ms) of each pulse (50 ms) were analyzed. To determine short-term synaptic transmission dynamics, each pulse in the 10 Hz train was normalized to the first pulse in both baseline and drug conditions.

Analysis of intrinsic physiological properties

Intrinsic excitability experiments were performed and analyzed as previous described [48, 49, 53, 64]. During current clamp experiments, membrane potentials were biased to −65 mV at the start of each sweep. Firing patterns were investigated using a series of 0.6 to 1-second current injections (step size 50 pA) until 400 pA was injected or depolarization block was induced. Spikes that did not have a peak voltage reaching at least −10 mV were not counted. F-I gain was the slope of a linear regression on the number of spikes at each current injection from 0 pA to the injection at which maximum firing frequency was attained, or 400pA, whichever came first. Total spike output was the sum of all spikes until maximum firing frequency or 400 pA. We used Python (version 3.10.4) to analyze all intrinsic properties, loading all ABF recording files with pyABF and using the packages NumPy, pandas, and matplotlib. For spike properties, we defined threshold as the voltage where the slope trajectory (dV/dT) reached 10 mV/ms. Amplitude was determined by the voltage difference between the threshold and the peak. Half-width was measured at the voltage corresponding to half the spike amplitude. Maximum rise slope was the maximum of dV/dt and maximum decay slope was the minimum of dV/dt. These properties were measured for the first spike evoked by the current injection. Adaptation index was computed at approximately twice the rheobase current from the 1-second current injection and was the number of spikes in the second half of the sweep subtracted from the number of spikes in the first half, divided by the total number of spikes. Input resistance (Rin), input capacitance (Cin), and membrane time constant (TC) were assessed with a series of small hyperpolarizing current steps (typically −10 to −20 pA). Rin was computed using the voltage difference between the maximum response during the current injection and the mean voltage of the 100 ms prior to the current injection, divided by the injected current. TC was computed by fitting an exponential decay curve to the voltage trace from the start of the current injection to the maximum voltage response. Input (membrane) capacitance (Cin) was calculated using the relationship Cin = TC/Rin. Hyperpolarizing current injection can produce a noticeable "sag" in some neurons, which indicates presence of a hyperpolarization-activated cation current (I_h) that activates after the initial hyperpolarization peak. Sag ratio was computed as the maximum response amplitude divided by the mean response amplitude of the last 50 ms of the current injection. Response amplitudes were computed relative to the baseline voltage, computed as the mean of the 100 ms prior to the current injection.

Analysis of transcriptomic data

We obtained MERFISH data from the Allen Institute for Brain Science's publicly available MERSCOPE v1 Whole Brain dataset [65]. This dataset's coronal slices are spaced 200 µm apart and are numbered in ascending order from posterior to anterior. We selected slice number 36 for visualization of retrosplenial cortex, slice 50 for anterior cingulate cortex, slice 33 for AD thalamus, and slice 31 for dorsal subiculum. The thalamic glutamatergic clusters corresponding to different nuclei identified in Yao et al., 2023 were used here. To enable analysis of dorsal subiculum, we restricted to clusters 384, 385, 386, 479, 481, 482 from slices 29 to 36.

We obtained snRNA-seq data from the Allen Institute's publicly available Mouse Whole Cortex and Hippocampus 10× dataset [66]. Using these identified clusters, we first analyzed expression of *Htr2a* in all glutamatergic neurons from each dissected cortical area. Next, we selected cells with

the region labels "RSP" and "ACA", to filter for cells from retrosplenial cortex and anterior cingulate cortex, respectively. For all violin plots and statistical comparisons, we grouped cells according to their existing cluster annotations. Cells were grouped into putative layers according to the layer annotation in their cluster label. We considered clusters with the following layer annotations as L2/3: ("L2 IT", "L2/3 IT"); these clusters as L5: ("L4 RSP-ACA", "L4 IT CTX", "L4/5 IT CTX", "L5 IT CTX", "L5 PT CTX", "L5 PPP", "L5/6 IT CTX", "L5/6 IT TPE-ENT"), and these clusters as L6 ("L6 IT CTX", "L6 IT ENTl", "L5/6 NP CTX", "L6 CT CTX", "L6b CTX", "Car3"). We additionally used the retrosplenial-specific cluster ("133_L2 IT RSPv-POST-PRE") as "L2/3 LR", based on previously identified correspondence of this transcriptomic cluster to the unique low rheobase (LR) neurons found in L2/3 of granular retrosplenial cortex [48, 49, 53, 54]. UMAPs were generated with the umap-learn package in Python.

Statistical analysis

Statistical analyses were performed in GraphPad Prism (version 10.0.1). Data were tested to determine whether they were normal, lognormal, or otherwise distributed. Spine counts and sEPSC frequency/amplitude distributions were found to be lognormally distributed, and were log transformed before statistical testing. All additional details on precise statistical tests used are provided in the figure legends.

Scientific illustrations

Illustrations for figures were created using Adobe Illustrator. The dendritic spine drawing used in the graphical abstract was modified from SciDraw (scidraw.io).

RESULTS

Psychedelics enhance synaptic connectivity in retrosplenial cortex

We first used multiplexed error-robust fluorescence in situ hybridization (MERFISH) and single-nucleus RNA sequencing (snRNA-seq) datasets [65, 66] to investigate expression of *Htr2a* in glutamatergic neurons across neocortical areas. We found that retrosplenial cortex (RSC) has the lowest *Htr2a* expression of the entire neocortex (Fig. 1A). In particular, the defining and most ubiquitous cells of the granular RSC (RSG) – the RSG-specific L2/3 low rheobase (LR) neurons [48, 49, 53, 54] – are almost entirely void of *Htr2a* expression (Fig. 1B, C). We repeated this analysis for ACC glutamatergic neurons and found widespread expression of *Htr2a* in L5 neurons (Fig. 1D, E). Population analyses confirmed that RSG LR neurons express very little *Htr2a* mRNA and ACC L5 neurons express a dramatically and significantly higher amount (Fig. 1F), consistent with previous work indicating high 5-HT_{2A} receptor expression in frontal cortex and low expression in retrosplenial cortex [32, 34–38].

Having identified that RSG L2/3 LR neurons lack expression of 5-HT_{2A} receptors, we asked if a single dose of the 5-HT_{2A} receptor-preferring psychedelic 25CN-NBOH (NBOH) [67–70] would result in a lasting enhancement of excitatory synaptic connectivity in these neurons (Fig. 2A). The current paradigm of psychedelic-induced plasticity suggests that psychedelics should not boost synaptic connectivity onto RSG LR neurons, as LR neurons do not express 5-HT_{2A} receptors [11–13, 21–30]. However, contrary to this prevailing theory, NBOH significantly increased the frequency of spontaneous excitatory postsynaptic currents (sEPSCs) in RSG LR neurons, recorded 2–3 days post-injection (Fig. 2B, C). Psychedelic-mediated enhancement of synaptic activity occurred at all doses tested (2, 10, 20 mg/kg; Supplementary Fig. 1). No changes were observed in the sEPSC amplitude or decay kinetics (Supplementary Fig. 1). As predicted from previous PFC experiments with psychedelics [23, 25, 28–30], NBOH also induced a lasting increase in the frequency of sEPSCs in ACC L5 RS neurons (Fig. 2D, E). NBOH-induced sEPSC frequency enhancement occurred with no dependence on sex in either RSG L2/3 LR neurons (Supplementary Fig. 2) or ACC L5 RS neurons (Supplementary Fig. 3). In addition, sEPSC frequencies were similar at both 2 and 3 days post-treatment (Supplementary Fig. 4). Thus, RSG LR neurons undergo psychedelic-induced synaptic boosting despite lacking 5-HT_{2A} receptors.

To determine if the NBOH-mediated glutamatergic synaptic elevation is accompanied by neuronal structural remodeling, we quantified the density of spines – the postsynaptic physical site of excitatory synapse formation – on basal and apical dendrites of RSG LR and ACC RS neurons using biocytin intracellular labeling. NBOH treatment significantly enhanced spine density in both RSG LR and ACC RS neurons (Fig. 2B–E). Interestingly, NBOH boosted only basal dendrite spine density in RSG LR neurons (Fig. 2C), potentially reflecting the potentiation of select inputs, such as those arising from the basal dendrite-targeting anterodorsal (AD) nucleus of the thalamus [49, 71, 72]. This contrasted with ACC RS neurons, which had both apical and basal spine density elevated (Fig. 2E). Taken together, psychedelic drugs can enhance synaptic connectivity of RSG neurons not expressing 5-HT_{2A} receptors in addition to its expected boost of synapses onto ACC L5 pyramidal cells.

We also examined if psychedelic treatment induces lasting changes to intrinsic excitability in addition to the synaptic changes observed. We found that the majority of RSG LR neuron passive and active intrinsic electrophysiological properties were unchanged from controls (Supplementary Fig. 5). We observed no lasting alterations of the intrinsic excitability of NBOH treated ACC L5 RS neurons (Supplementary Fig. 6), in alignment with previous PFC studies on psychedelic drugs [27, 29]. Thus, treatment with a single psychedelic dose induces a lasting enhancement of excitatory synaptic connectivity in 5-HT_{2A} receptor-lacking RSG LR neurons but leaves intrinsic excitability largely unaffected.

Thalamic inputs to RSG express functional presynaptic 5-HT_{2A} receptors

Having found that psychedelics enhance synaptic connectivity onto 5-HT_{2A} receptor-lacking RSG L2/3 LR neurons, we hypothesized that this boost could depend on 5-HT_{2A} receptor expression on presynaptic inputs to LR neurons. Therefore, we next analyzed 5-HT_{2A} receptor expression in long-range excitatory inputs to RSG LR neurons. While granular retrosplenial cortex receives glutamatergic long-range inputs from a wide variety of cortical and subcortical sources, we have shown that LR neurons are only strongly innervated by two primary glutamatergic sources: anterior thalamus and dorsal subiculum [49] (Supplementary Fig. 7). Using MERFISH [65] and RNA sequencing (Thalamoseq) [73] datasets, we analyzed *Htr2a* mRNA in glutamatergic thalamic nuclei (Fig. 3A; Supplementary Fig. 8). We found that the anterodorsal nucleus (AD) strongly expresses *Htr2a* (Fig. 3B), with higher expression levels than all other thalamic nuclei (Fig. 3C; Supplementary Fig. 8A). We confirmed selective expression of *Htr2a* in AD thalamus using fluorescent in situ hybridization (RNAScope) experiments (Supplementary Fig. 8B). We next repeated the MERFISH analysis with dorsal subiculum glutamatergic neurons and found overall very little *Htr2a* expression (Supplementary Fig. 9A, B). Together, this combination of connectivity and transcriptomic analyses led us to the hypothesis that long-range inputs onto RSG LR cells specifically from AD thalamic cells expressing *Htr2a* are likely to be the synapses boosted by psychedelic drugs (Supplementary Fig. 9C).

To determine if AD axons synapsing onto RSG LR neurons express functional presynaptic 5-HT_{2A} receptors, we utilized pharmacology in combination with channelrhodopsin-assisted circuit mapping (Fig. 3D–F). We first recorded RSG L2/3 LR neurons while stimulating L3 anterior thalamic axons (disconnected from cell bodies), which reflect AD inputs due to the strong synaptic targeting of L3 by AD axons [46, 49, 71, 72], and found that RSG LR neurons receive strong monosynaptic input, able to drive spiking

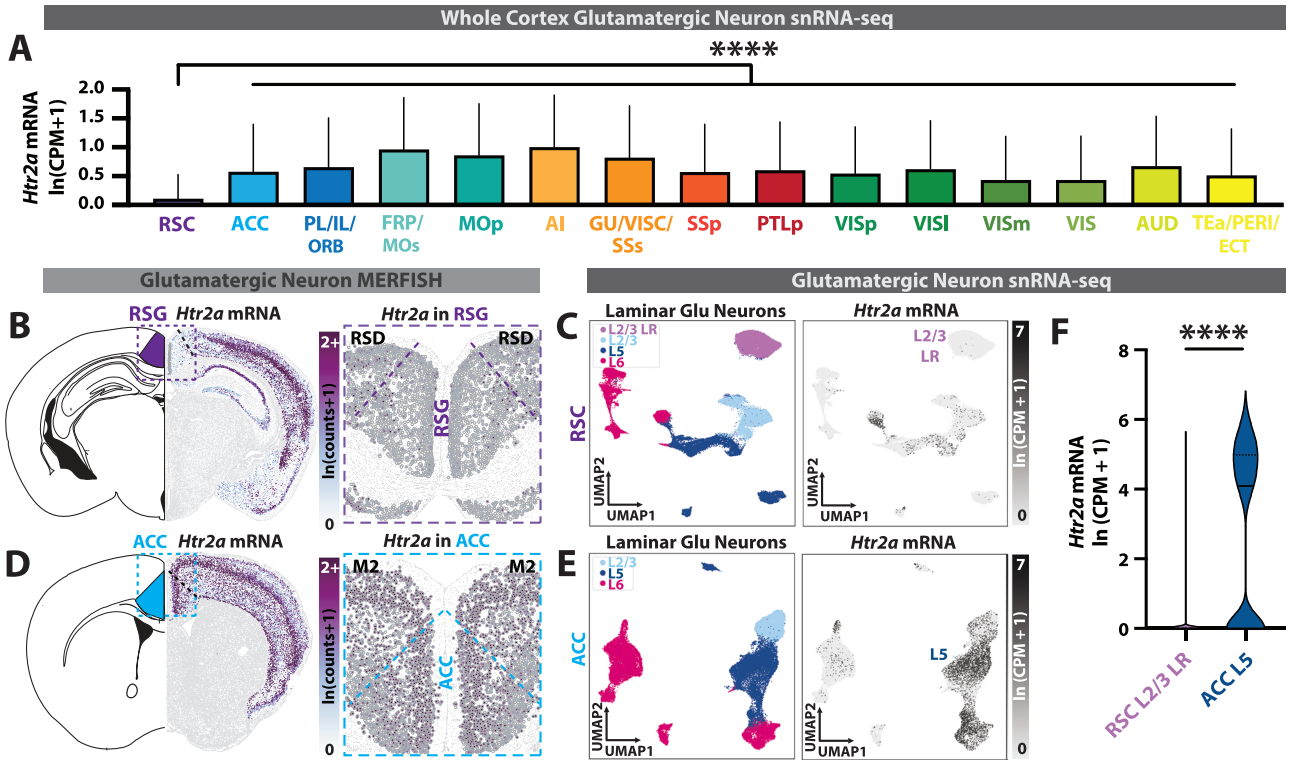

Fig. 1 Identification of 5-HT$_{2A}$R-lacking neocortical glutamatergic neurons. A *Htr2a* mRNA expression (snRNA-seq) in glutamatergic neurons across neocortical areas. Retrosplenial cortex expresses significantly less *Htr2a* mRNA than all other areas ($F_{(14,\ 810387)} = 4019$, $P < 10^{-15}$, one-way ANOVA; for multiple comparisons with Dunnett correction between retrosplenial (RSC) and every other cortical area, $P < 10^{-9}$). **B** *Left*, Schematic of a coronal slice containing granular retrosplenial cortex (RSG). *Right*, *Htr2a* mRNA expression in retrosplenial glutamatergic neurons from a representative MERFISH section. Note the lack of *Htr2a* expression in RSG L2/3 neurons. **C** *Left*, UMAP of retrosplenial glutamatergic neurons from snRNA-seq and color-coded by layer. *Right*, expression of *Htr2a* mRNA in retrosplenial glutamatergic neurons. **D** *Left*, schematic of a coronal slice containing anterior cingulate cortex (ACC, blue). *Right*, expression of Htr2a mRNA in anterior cingulate (ACC) glutamatergic neurons from a representative MERFISH section. **E** *Left*, UMAP of ACC glutamatergic neurons from snRNA-seq, color-coded by layer. *Right*, *Htr2a* mRNA expression in ACC glutamatergic neurons. Note the high expression in ACC L5 neurons. **F** RSG LR glutamatergic neurons express significantly less *Htr2a* mRNA compared to ACC L5 glutamatergic neurons ($t_{(30535)} = 98.2$, $P < 10^{-15}$, two-tailed unpaired t-test). MERFISH and snRNA-seq data sourced from Allen Institute databases [65, 66]. Bar plots represent mean + standard deviation. ****: $P < 0.0001$.

(Fig. 3G). We next recorded optogenetic-evoked excitatory postsynaptic currents (oEPSCs) from AD axons in RSG LR neurons, and subsequently bath-applied NBOH for 10 min while continuing to record AD-evoked currents (Supplementary Fig. 10A). We found that NBOH acutely increased AD→RSG LR oEPSC amplitude and modulated short-term synaptic transmission dynamics (Fig. 3H; Supplementary Fig. 10A, B). In addition, NBOH acutely increased the frequency of spontaneous EPSCs (sEPSCs) in RSG LR neurons (Fig. 3I, J).

Htr2a-expressing AD thalamus neurons could have 5-HT$_{2A}$Rs in distinct cellular compartments, such as somatodendritic areas and/or axon terminals (presynaptic to RSG LR neurons) and could thus modulate different aspects of cellular neurophysiology [74]. To next determine if AD neurons express functional somatodendritic 5-HT$_{2A}$ receptors, we directly recorded from AD neurons' cell bodies and bath-applied NBOH (Supplementary Fig. 11A). We found that the intrinsic somatodendritic properties of AD neurons were unresponsive to psychedelic modulation of intrinsic excitability. NBOH did not significantly alter resting membrane potentials (RMP) or evoked firing rates of AD neurons (Supplementary Fig. 11B–D), in contrast to cell types in other brain regions expressing somatodendritic 5-HT$_{2A}$ receptors [29, 75–78], but consistent with prior somatic recordings of AD neurons revealing no effect of DOI [79]. Thus, AD neurons do not express functional somatodendritic 5-HT$_{2A}$ receptors. Additionally, NBOH had no impact on sEPSC frequency recorded in AD neurons (Supplementary Fig. 11E, F), indicating a lack of presynaptic 5-HT$_{2A}$ receptors in the inputs to AD.

Thus, AD neurons lack functional somatodendritic 5-HT$_{2A}$ receptors, but AD axons which target RSG LR neurons express functional 5-HT$_{2A}$ receptors presynaptic to LR neurons, which enhance glutamatergic synaptic transmission upon acute activation. In addition, as shown in Fig. 2, psychedelics induce a lasting increase in excitatory synaptic connections in postsynaptic 5-HT$_{2A}$ receptor-lacking RSG LR neurons. Are the presynaptic AD thalamic 5-HT$_{2A}$ receptors required to induce this long-lasting psychedelic boost of synaptic inputs onto LR neurons in RSG (Fig. 3K, L)? This is the question we next answered by engineering a new conditional knockout mouse line.

Htr2a conditional knockout reveals role of presynaptic 5-HT$_{2A}$ receptors for psychedelic-induced synaptic enhancement

To selectively manipulate 5-HT$_{2A}$ receptors, we created and functionally validated an *Htr2a* conditional knockout (cKO) mouse line using Crispr-Cas9 technology (Fig. S12; Table 1). Upon introduction of the Cre protein into specific regions or cells, the dual-'floxed' *Htr2a* (*Htr2a*$^{fl/fl}$) gene produces dysfunctional mRNA, which results in 5-HT$_{2A}$ receptor elimination (Fig. 4A). We bilaterally delivered Cre/GFP to AD thalamic neurons of *Htr2a*$^{fl/fl}$ mice to create mice that selectively lack AD 5-HT$_{2A}$ receptors (Fig. 4B).

To determine if 5-HT$_{2A}$ receptors located on AD axons are responsible for the acute enhancement of spontaneous excitatory

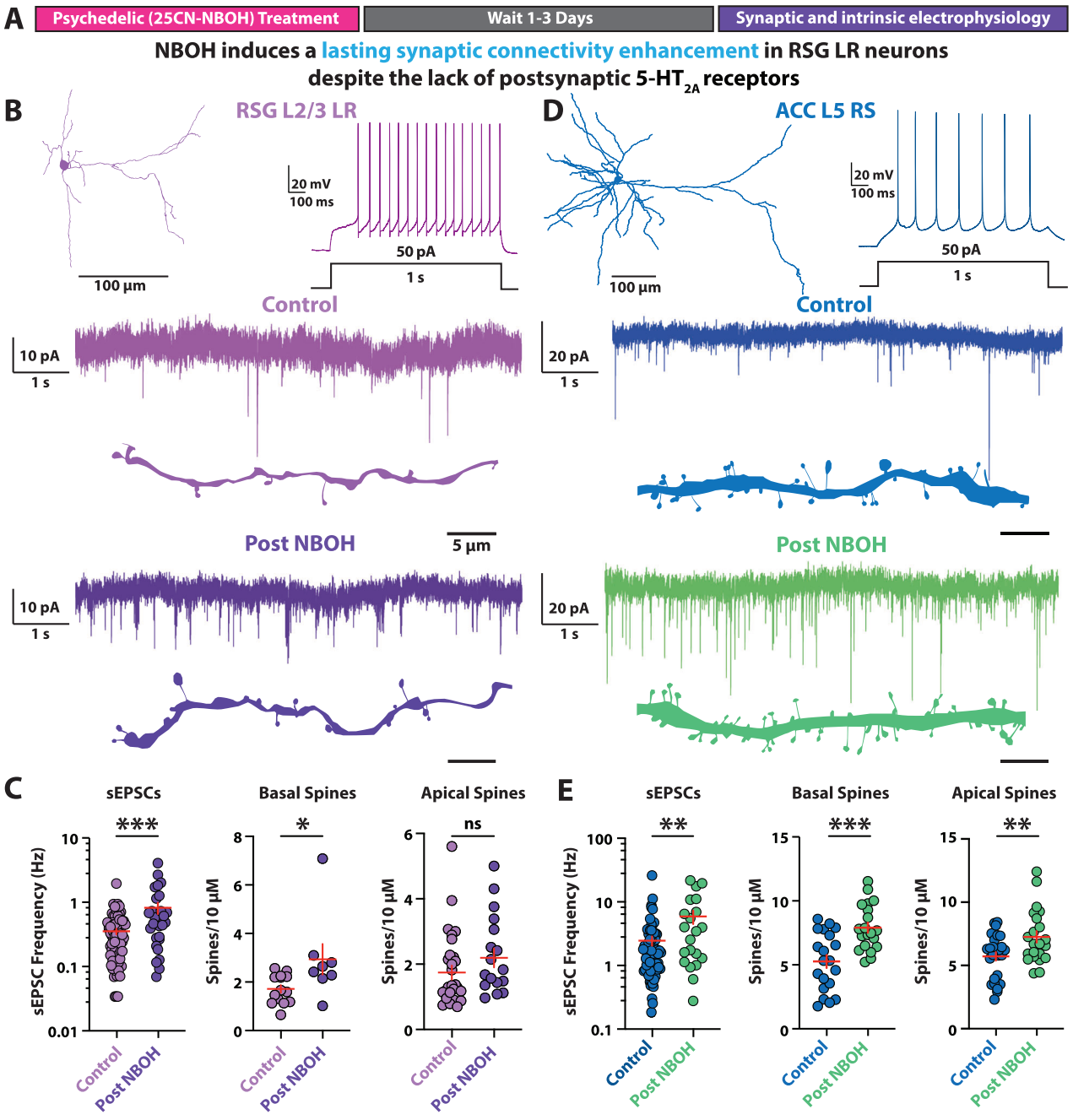

Fig. 2 Psychedelic-induced synaptic enhancement onto neocortical neurons. A Experimental timeline. Mice are given a single dose of 25CN-NBOH (2 mg/kg) via intraperitoneal (IP) injection. After 1–3 days acute brain slices are taken and intrinsic and synaptic electrophysiology properties of RSG L2/3 LR pyramidal neurons and ACC L5 RS pyramidal neurons are recorded. **B** *Top*, RSG LR neuron morphological reconstruction and voltage trace showing firing pattern of RSG L2/3 LR pyramidal neuron. *Bottom*, current trace showing spontaneous excitatory postsynaptic currents (sEPSCs) and dendritic spine tracings of control (violet) and NBOH (dark purple) treated LR neurons. **C** NBOH treatment significantly increases LR sEPSC frequency (*left*; $t_{(99)} = 3.552$, SEM Control = 0.0357, SD Control = 0.3032, SEM Drug = 0.0872, SD Drug = 0.4930, P = 0.0006, two-tailed unpaired t test) and density of basal dendrite spines (*middle*; $t_{(20)} = 2.392$, SEM Control = 0.1590, SD Control = 0.5950, SEM Drug = 0.6314, SD Drug = 1.786, P = 0.0267, two-tailed unpaired t test), but not apical dendrite spines (*right*; $t_{(42)} = 1.502$, SEM Control = 0.2181, SD Control = 1.133, SEM Drug = 0.2933, SD Drug = 1.210, P = 0.1405, two-tailed unpaired t test). **D** *Top*, recording schematic, voltage trace showing firing pattern of ACC L5 RS pyramidal neuron. *Bottom*, Current trace showing ACC L5 RS sEPSCs and dendritic spine tracings before (blue) and after (green) NBOH treatment. (**E**) NBOH treatment significantly increases ACC L5 RS sEPSC frequency (*left*; $t_{(91)} = 2.934$, SEM Control = 0.4049, SD Control = 3.436, SEM Drug = 1.408. SD Drug = 6.453, P = 0.0042, two-tailed unpaired t test) and density of basal (*middle*; $t_{(38)} = 3.957$, SEM Control = 0.5084, SD Control = 2.274, SEM Drug = 0.4030, SD Drug = 1.802, P = 0.0003., two-tailed unpaired t test) and apical (*right*; $t_{(47)} = 2.746$, SEM Control = 0.3360, SD Control = 1.746, SEM Drug = 0.4556, SD Drug = 2.137, P = 0.0085, two-tailed unpaired t test) dendritic spines. Error bars represent mean +/- standard error of the mean (SEM). *p < 0.05; **p < 0.01; ***p < 0.001; ns, not significant.

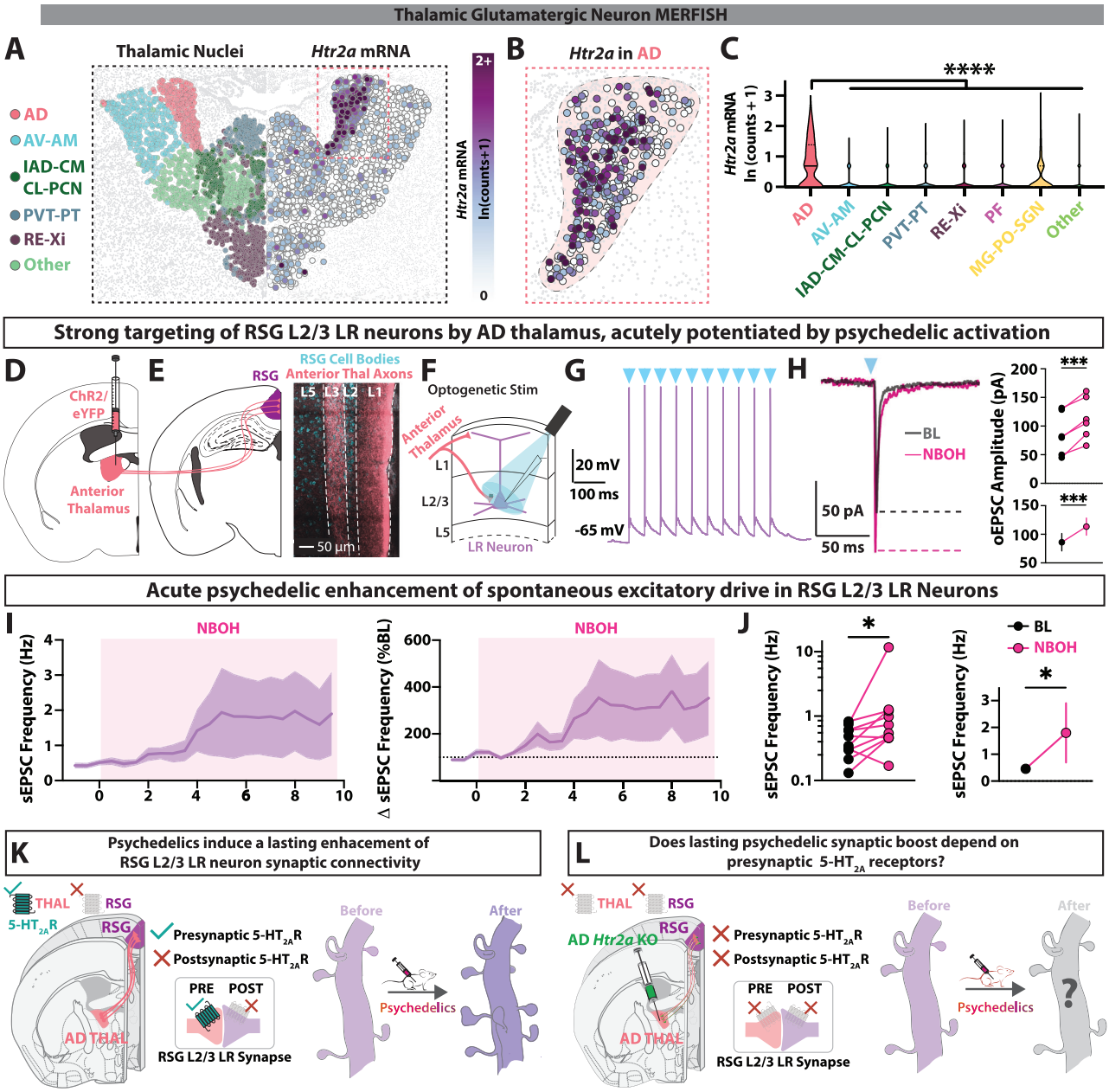

Fig. 3 Anterodorsal thalamic cells projecting to retrosplenial cortex express 5-HT$_{2A}$Rs. A MERFISH section showing thalamic glutamatergic neurons color mapped by thalamic nucleus (*left*) and *Htr2a* mRNA expression (*right*). **B** Increased magnification showing *Htr2a* expression in the anterodorsal nucleus of each hemisphere. **C** Violin plot of MERFISH glutamatergic thalamic nuclei; Anterodorsal (AD) nucleus contains significantly more *Htr2a* mRNA than all other thalamic nuclei ($F_{(7,\ 58774)} = 896.1$, $P < 10^{-15}$, one-way ANOVA; for multiple comparisons with Dunnett correction between AD and every thalamic nucleus/group, $P < 10^{-15}$). **D** *Right*, schematic of a brain slice containing anterior thalamic nuclei (ANT) with intracranial viral delivery of channelrhodopsin (ChR2) and enhanced yellow fluorescent protein (eYFP, pseudocolored pink here). **E** *Left*, schematic of a brain slice containing RSG. *Right*, anterior thalamic axons in RSG after intracranial viral delivery of ChR2 and eYFP into anterior thalamus. **F** Experimental recording schematic: RSG LR neurons are recorded using whole-cell electrophysiology while stimulating ChR2-expressing anterior thalamic axons. **G** Current-clamp spiking response of LR neuron upon AD axonal stimulation (L3 axon stimulation; blue triangles represent time of light pulses). **H** *Left*, Voltage-clamp response of LR neuron upon AD ChR2 stimulation before and after a 10-min perfusion with NBOH (10 µM). *Right*, quantification of baseline and in-drug AD-evoked EPSC amplitude ($t_{(5)} = 8.307$, SEM Baseline = 15.22, SD Baseline = 37.28, SEM Drug = 15.01, SD Drug = 36.78, $P = 0.0004$, two-tailed paired t test). **I** Acute NBOH increases the frequency of sEPSCs in LR neurons. sEPSC frequency across time is presented as overall frequency (Hz, left) and as percentage of baseline sEPSC frequencies (%BL, left). **J** sEPSC frequency is significantly elevated with acute NBOH application ($t_{(10)} = 2.920$, Baseline SEM = 0.0738, Baseline SD = 0.2333, Drug SEM = 1.109, Drug SD = 3.507, $P = 0.0137$, two-tailed paired t test between baseline and drug. **K** Summery of findings so far. *Left*, RSG LR neurons lack 5-HT$_{2A}$ receptors, but AD inputs to these neurons express presynaptic 5-HT$_{2A}$ receptors. *Right*, psychedelic treatment enhances synaptic connectivity of LR neurons. **L** Hypothesis to be tested next: does genetic elimination of presynaptic 5-HT$_{2A}$ receptors of AD thalamus neurons abolish psychedelic-induced neuroplasticity in RSG LR neurons? snRNA-seq data are adapted from the Allen Institute [65]. Error bars represent mean +/− standard error of the mean (SEM).*p < 0.05; ***p < 0.001; ****p < 0.0001; ns, not significant.

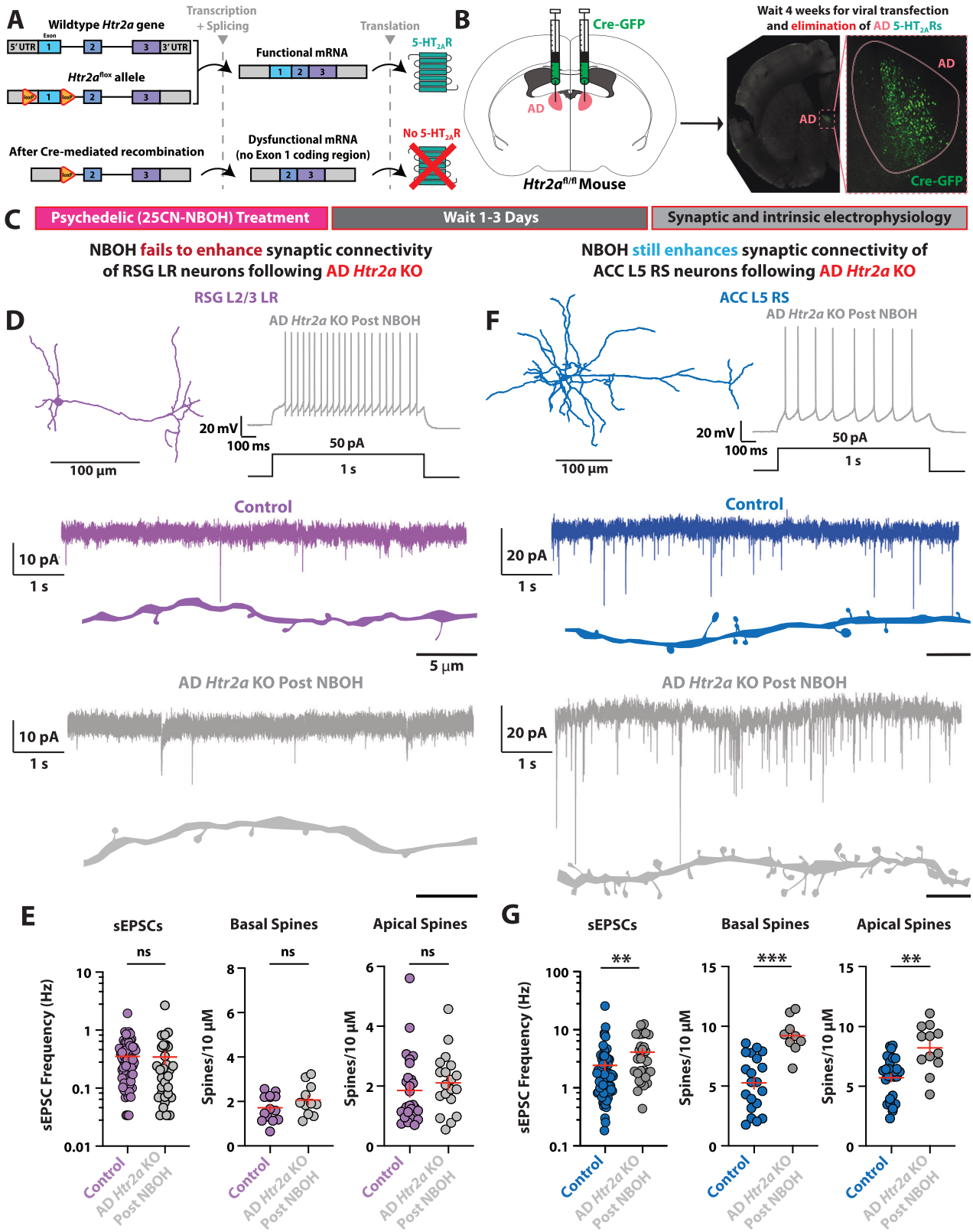

drive in RSG L2/3 LR neurons, we next recorded from RSG LR cells from brain slices lacking AD 5-HT$_{2A}$ receptors (Supplementary Fig. 13A). We found that NBOH did not significantly enhance sEPSC frequency after loss of AD 5-HT$_{2A}$ receptors (Supplementary Fig. 13B, C). Therefore, AD axonal 5-HT$_{2A}$ receptors are responsible for acute psychedelic enhancement of spontaneous excitatory drive in RSG L2/3 LR neurons.

We then administered a single dose of NBOH (2 mg/kg, IP), waited 1–3 days, and then conducted whole-cell electrophysiology experiments in RSG LR neurons (Fig. 4C). We found that

Fig. 4 Presynaptic 5-HT$_{2A}$Rs are required for psychedelic synaptic enhancement onto retrosplenial neurons lacking postsynaptic 5-HT$_{2A}$Rs. A Strategy for manipulation of *Htr2a* gene. Schematic of *Htr2a* of wildtype (*top*), floxed allele insertion before the presence of Cre (*middle*), and after Cre-mediated recombination (*bottom*). Upon recombination, the *Htr2a* gene is unable to create viable mRNA, and 5-HT$_{2A}$ receptor expression is lost. **B** Schematic of dual-hemisphere intracranial viral delivery of Cre and green fluorescent protein (GFP) to AD nucleus of dual-floxed *Htr2a* transgenic mice (*left*), and expression of GFP in AD neurons after transfection (*right*) **C** Experimental timeline. Mice lacking *Htr2a* expression in AD thalamus are given a single dose of 25CN-NBOH (2 mg/kg) via intraperitoneal (IP) injection. After 1–3 days, intrinsic and synaptic electrophysiology properties of RSG L2/3 LR pyramidal neurons and ACC L5 RS pyramidal neurons are recorded. **D** *Top*, LR neuron morphological reconstruction (*left*) and firing pattern after AD *Htr2a* elimination followed by psychedelic treatment (*right*). *Bottom*, sEPSCs of control (violet) and after NBOH treatment in AD *Htr2a* KO (grey) LR neurons. **E** NBOH treatment fails to increase LR sEPSC frequency (*left*; $t_{(102)} = 1.559$, SEM Control = 0.0357, SD Control = 0.3032, SEM Drug = 0.0872, SD Drug = 0.4930, P = 0.1221, two-tailed unpaired t test), basal dendrite spines (*middle*; $t_{(23)} = 1.330$, SEM Control = 0.1590, SD Control = 0.5950, SEM Drug = 0.2081, SD Drug = 0.6902, P = 0.1965, two-tailed unpaired t test), or apical dendrite spines (*right*; $t_{(44)} = 0.988$, SEM Control = 0.2181, SD Control = 1.133, SEM Drug = 0.2269, SD Drug = 0.9892, P = 0.3286, two-tailed unpaired t test) after AD *Htr2a* elimination. **F** *Top*, ACC L5 RS neuron morphological reconstruction (*left*) and firing pattern after AD thalamus *Htr2a* elimination followed by psychedelic treatment. *Bottom*, sEPSCs of control (violet) and after NBOH treatment in AD *Htr2a* KO (grey) LR neurons. **G** NBOH treatment still significantly increases ACC L5 RS sEPSC frequency (*left*; $t_{(100)} = 3.359$, SEM Control = 0.4049, SD Control = 3.436, SEM Drug = 0.6222. SD Drug = 3.408, P = 0.0011, two-tailed unpaired t test), basal spines (*middle*; $t_{(27)} = 3.758$, SEM Control = 0.5084, SD Control = 2.274, SEM Drug = 0.5008, SD Drug = 1.052, P = 0.0008, two-tailed unpaired t test), and apical spines (*right*; $t_{(37)} = 3.359$, SEM Control = 0.3360, SD Control = 1.746, SEM Drug = 0.5728, SD Drug = 1.984, P = 0.0018, two-tailed unpaired t test) after AD *Htr2a* elimination. Error bars represent mean +/− standard error of the mean (SEM).*p < 0.05; **p < 0.01; ***p < 0.001; ns, not significant.

elimination of AD thalamic 5-HT$_{2A}$ receptors prevented the psychedelic NBOH from enhancing sEPSC frequency in RSG LR neurons (Fig. 4D, E). This effect was seen in both male and female mice (Supplementary Fig. 14). In contrast, NBOH still significantly enhanced sEPSC frequency in ACC L5 RS neurons following AD thalamic 5-HT$_{2A}$ receptor removal (Fig. 4F, G), consistent with the lack of AD thalamic input to ACC [72] and highlighting the synapse-specificity of the conditional knockout strategy. There were no significant changes to sEPSC amplitude or kinetics of RSG LR or ACC RS neurons (Supplementary Fig. 15).

Next, we analyzed dendritic spine density in AD *Htr2a*-KO RSG L2/3 LR and ACC L5 RS neurons following NBOH treatment and compared these to control neurons. NBOH did not increase RSG LR spine density following AD *Htr2a* elimination (Fig. 4D, E). However, NBOH still significantly increased spine density in ACC RS neurons (Fig. 4F, G). Therefore, presynaptic AD thalamic 5-HT$_{2A}$ receptors are required for psychedelic-mediated synaptic enhancement in RSG LR neurons that lack postsynaptic 5-HT$_{2A}$ receptors. Finally, we analyzed intrinsic membrane and firing properties and found that most intrinsic electrophysiological properties were unchanged in RSG LR (Supplementary Fig. 16) and ACC RS neurons in cKO animals after NBOH treatment (Supplementary Fig. 17). Future experiments, beyond the scope of this study, utilizing conditional knockouts of serotonin receptors selectively in neurons that exclusively express somatodendritic 5-HT$_{2A}$ receptors (but lack 5-HT$_{2A}$ receptors in their axons/terminals) will provide additional insight into the regulation of cellular and synaptic neurophysiology by psychedelic drugs. Experiments such as those utilized here and elsewhere [23–25, 28–30, 80, 81] will help to systematically identify such neurons.

In conclusion, psychedelics can enhance synaptic connectivity onto RSG pyramidal neurons despite the lack of 5-HT$_{2A}$ receptors on these cells. This psychedelic-induced synaptic boost in retrosplenial cortex requires presynaptic 5-HT$_{2A}$ receptors in AD thalamic input neurons.

DISCUSSION

Enhancement of neuroplasticity – initiated through signaling cascades caused by postsynaptic or intracellular 5-HT$_{2A}$ receptor activation – is thought to be a key neurobiological mechanism underlying psychedelic treatment of neuropsychiatric disorders. Based on this understanding, neurons lacking 5-HT$_{2A}$ receptors should not undergo psychedelic-induced synapse formation [11–13, 21–30]. Here, we instead show that psychedelics can also enhance synaptic connections in cortical pyramidal neurons that lack 5-HT$_{2A}$ receptors (Figs. 1–3), and that this form of psychedelic plasticity requires presynaptic axonal 5-HT$_{2A}$ receptor activation (Fig. 4).

5-HT$_{2A}$ receptors can be located postsynaptically on somatodendritic or intracellular compartments, or presynaptically on axon terminals [28, 32, 82, 83]. This location determines the precise excitability-modulating signaling cascades that are triggered by activation of 5-HT$_{2A}$ receptors. Postsynaptic (somatodendritic) 5-HT$_{2A}$ receptor activation induces several changes to neuronal electrophysiology, including suppression and inactivation of voltage-gated transient sodium channels [84, 85], resting membrane potential depolarization [35–38, 77] and depression of AMPA receptors [83]. In contrast, activation of axonal 5-HT$_{2A}$ receptors induces blockade of the voltage-gated potassium channel Kv1.2, which increases excitability within axon terminals and facilitates increased excitatory glutamate release [82, 86, 87] (Fig. 3H; Supplementary Fig. 10). However, also see reference [77] for somatodendritic depolarization-mediated enhancement of sEPSC frequency. Our results show that a long-term consequence of psychedelic activation of presynaptic 5-HT$_{2A}$ receptors is to boost synaptic activity and spine formation onto postsynaptic neurons, even when the postsynaptic neuron does not express 5-HT$_{2A}$ receptors.

Only 26% of neurons in the mouse brain express detectable 5-HT$_{2A}$ receptor mRNA (Supplementary Fig. 18) [65]. However, neurons typically connect to thousands of other neurons [88], indicating that many neurons lacking postsynaptic 5-HT$_{2A}$ receptors are likely to receive at least some inputs from presynaptic neurons that do express 5-HT$_{2A}$ receptors. Thus, the mechanistic understanding of psychedelic plasticity presented here widens the therapeutic application of psychedelic drugs. Enhancing synaptic connectivity in the retrosplenial cortex is a key example of this therapeutic potential, as RSG pyramidal neurons lack 5-HT$_{2A}$ receptors, but are strongly innervated by 5-HT$_{2A}$ receptor-expressing AD thalamic inputs. AD thalamus contains vestibular-dependent head direction cells, which relay this directional information to the dendrites of RSG LR neurons. These inputs are relevant to memory, vestibular-dependent spatial processing, spatial orientation, awareness, and attention [43, 49, 71, 72, 89–93]. Theoretical and experimental work shows that this synapse from AD to RSG neurons is important for supporting angular velocity encoding in the RSG, a key component of the path integration computations required to support successful spatial navigation and orientation [49, 90, 92, 94, 95]. Thus, psychedelics may have promise in treating circuit disorders involving the synapses between the anterior thalamus and retrosplenial cortex, including Alzheimer's

disease, diencephalic amnesia, wandering syndrome, and impaired extinction of fearful memories [55–61, 91–93, 96–98].

The newly created and validated *Htr2a* conditional knockout line enables the possibility of many future studies on the importance of 5-HT_{2A} receptors in mediating psychedelic-induced plasticity across the brain. This will allow the testing of novel hypotheses on the region-, cell-type-, and cellular compartment-specific functions of 5-HT_{2A} receptors, resulting in a better understanding of 5-HT_{2A} receptor physiological function and psychedelic control of neural plasticity. Such studies will help to rationally and mechanistically support the application of psychedelic drugs to treat specific disorders and will likely continue to reveal that psychedelic drugs impact far more neural circuits in the brain than previously appreciated. This promises more avenues for psychedelic treatment than currently predicted, but also suggests the need to be wary of actions on previously unexpected synapses.

DATA AVAILABILITY

Data and code required to generate the figures in this manuscript are available from the corresponding author upon reasonable request. The new conditional *Htr2a* knockout mouse line is available from the corresponding author upon reasonable request.

REFERENCES

1. Brouns EJ, Ekins TG, Ahmed OJ Single-dose psychedelic enhances cognitive flexibility and reversal learning in mice weeks after administration. Psychedelics 2025;1–7. https://doi.org/10.61373/pp025r.0002.
2. Bogenschutz MP, Forcehimes AA, Pommy JA, Wilcox CE, Barbosa P, Strassman RJ. Psilocybin-assisted treatment for alcohol dependence: a proof-of-concept study. J Psychopharmacol. 2015;29:289–99.
3. Johnson MW, Garcia-Romeu A, Cosimano MP, Griffiths RR. Pilot study of the 5-HT2AR agonist psilocybin in the treatment of tobacco addiction. J Psychopharmacol. 2014;28:983–92.
4. Sanches RF, de Osório FL, dos Santos RG, Macedo LRH, Maia-de-Oliveira JP, Wichert-Ana L, et al. Antidepressant effects of a single dose of ayahuasca in patients with recurrent depression. J Clin Psychopharm. 2016;36:77–81.
5. Carhart-Harris RL, Bolstridge M, Rucker J, Day CMJ, Erritzoe D, Kaelen M, et al. Psilocybin with psychological support for treatment-resistant depression: an open-label feasibility study. Lancet Psychiatry. 2016;3:619–27.
6. Carhart-Harris RL, Bolstridge M, Day CMJ, Rucker J, Watts R, Erritzoe DE, et al. Psilocybin with psychological support for treatment-resistant depression: six-month follow-up. Psychopharmacology. 2018;235:399–408.
7. Palhano-Fontes F, Barreto D, Onias H, Andrade KC, Novaes MM, Pessoa JA, et al. Rapid antidepressant effects of the psychedelic ayahuasca in treatment-resistant depression: a randomized placebo-controlled trial. Psychol Med. 2019;49:655–63.
8. Doss MK, Považan M, Rosenberg MD, Sepeda ND, Davis AK, Finan PH, et al. Psilocybin therapy increases cognitive and neural flexibility in patients with major depressive disorder. Transl Psychiat. 2021;11:574.
9. Carhart-Harris R, Giribaldi B, Watts R, Baker-Jones M, Murphy-Beiner A, Murphy R, et al. Trial of psilocybin versus escitalopram for depression. New Engl J Med. 2021;384:1402–11.
10. Goodwin GM, Aaronson ST, Alvarez O, Arden PC, Baker A, Bennett JC, et al. Single-dose psilocybin for a treatment-resistant episode of major depression. N Engl J Med. 2022;387:1637–48.
11. Savalia NK, Shao L-X, Kwan AC. A dendrite-focused framework for understanding the actions of ketamine and psychedelics. Trends Neurosci. 2021;44:260–75. https://doi.org/10.1016/j.tins.2020.11.008.
12. Kwan AC, Olson DE, Preller KH, Roth BL. The neural basis of psychedelic action. Nat Neurosci. 2022;25:1407–19.
13. Olson DE. Biochemical mechanisms underlying psychedelic-induced neuroplasticity. Biochemistry. 2022;61:127–36.
14. Nichols DE. Psychedelics. Pharmacol Rev. 2016;68:264–355.
15. Isbell H. Comparison of the reactions induced by psilocybin and LSD-25 in man. Psychopharmacologia. 1959;1:29–38.
16. Wolbach AB, Isbell H, Miner EJ. Cross tolerance between mescaline and LSD-25 with a comparison of the mescaline and LSD reactions. Psychopharmacologia. 1962;3:1–14.
17. Leary T, Litwin G, Metzner R. Reactions to psilocybin administered in a supportive environment. J Nerv Ment Dis. 1963;137:561–73. https://doi.org/10.1097/00005053-196312000-00007.
18. Rosenberg DE, Isbell H, Miner EJ, Logan CR. The effect of N,N-dimethyltryptamine in human subjects tolerant to lysergic acid diethylamide. Psychopharmacologia. 1964;5:217–27.
19. Shulgin AT. Profiles of psychedelic drugs - psilocybin. J Psychoactive Drugs. 1980;12:79–79.
20. Strassman R, Qualls CR, Uhlenhuth EH, Kellner R. Dose-Response Study of N,N-Dimethyltryptamine II. Archives of General Psychiatry. 1994;51:98–108.
21. Slocum ST, DiBerto JF, Roth BL. Molecular insights into psychedelic drug action. J Neurochem. 2022;162:24–38. https://doi.org/10.1111/jnc.15540
22. McClure-Begley TD, Roth BL. The promises and perils of psychedelic pharmacology for psychiatry. Nat Rev Drug Discov. 2022;21:463–73.
23. Ly C, Greb AC, Cameron LP, Wong JM, Barragan EV, Wilson PC, et al. Psychedelics promote structural and functional neural plasticity. Cell Reports. 2018;23:3170–82.
24. Cameron LP, Tombari RJ, Lu J, Pell AJ, Hurley ZQ, Ehinger Y, et al. A non-hallucinogenic psychedelic analogue with therapeutic potential. Nature. 2021;589:474–9.
25. Shao L-X, Liao C, Gregg I, Davoudian PA, Savalia NK, Delagarza K, et al. Psilocybin induces rapid and persistent growth of dendritic spines in frontal cortex in vivo. Neuron. 2021;109:2535–2544.e4. https://doi.org/10.1016/j.neuron.2021.06.008
26. Revenga M, de la F, Zhu B, Guevara CA, Naler LB, Saunders JM, et al. Prolonged epigenomic and synaptic plasticity alterations following single exposure to a psychedelic in mice. Cell Reports. 2021;37:109836.
27. Cameron LP, Patel SD, Vargas MV, Barragan EV, Saeger HN, Warren HT, et al. 5-HT2ARs mediate therapeutic behavioral effects of psychedelic tryptamines. ACS Chem Neurosci. 2023;14:351–8.
28. Vargas MV, Dunlap LE, Dong C, Carter SJ, Tombari RJ, Jami SA, et al. Psychedelics promote neuroplasticity through the activation of intracellular 5-HT2A receptors. Science. 2023;379:700–6.
29. Ekins TG, Brooks I, Kailasa S, Rybicki-Kler C, Jedrasiak-Cape I, Donoho E, et al. Cellular rules underlying psychedelic control of prefrontal pyramidal neurons. bioRxiv:2023.10.20.563334. 2023. https://doi.org/10.1101/2023.10.20.563334.
30. Shao L-X, Liao C, Davoudian PA, Savalia NK, Jiang Q, Wojtasiewicz C, et al. Pyramidal cell types and 5-HT2A receptors are essential for psilocybin's lasting drug action. Nature. 2025;642:411–20. https://doi.org/10.1038/s41586-025-08813-6.
31. Willins DL, Deutch AY, Roth BL. Serotonin 5-HT2A receptors are expressed on pyramidal cells and interneurons in the rat cortex. Synapse. 1997;27:79–82.
32. Jakab RL, Goldman-Rakic PS. 5-hydroxytryptamine 2A serotonin receptors in the primate cerebral cortex: possible site of action for hallucinogenic and antipsychotic drugs in pyramidal cell apical denderites. Proc Natl Acad Sci USA. 1998;95:735–40.
33. Cornea-Herbert V, Riad M, Wu C, Singh SK, Descarries L. Cellular and subcellular distribution of the serotonin 5-ht2a receptor in the central nervous system of adult rat. J Comp Neurol. 1999;409:187–209.
34. Weber ET, Andrade R. Htr2a gene and 5-HT2A receptor expression in the cerebral cortex studied using genetically modified mice. Front Neurosci-Switz. 2010;4:36.
35. Avesar D, Gulledge AT. Selective serotonergic excitation of callosal projection neurons. Front Neural Circuit. 2012;6:12.
36. Stephens EK, Baker AL, Gulledge AT. Mechanisms underlying serotonergic excitation of callosal projection neurons in the mouse medial prefrontal cortex. Front Neural Circuit. 2018;12:2.
37. Stephens EK, Avesar D, Gulledge AT. Activity-dependent serotonergic excitation of callosal projection neurons in the mouse prefrontal cortex. Front Neural Circuit. 2014;8:97.
38. Avesar D, Stephens EK, Gulledge AT. Serotonergic regulation of corticoamygdalar neurons in the mouse prelimbic cortex. Front Neural Circuit. 2018;12:63.
39. Ploski JE, Vaidya VA. The neurocircuitry of PTSD and major depression: insights into overlapping and distinct circuit dysfunction - a tribute to ron duman. Biol Psychiat. 2021;90:109–17.
40. Giustino TF, Maren S. The role of the medial prefrontal cortex in the conditioning and extinction of fear. Front Behav Neurosci. 2015;9:298.
41. Zaretsky TG, Jagodnik KM, Barsic R, Antonio JH, Bonanno PA, MacLeod C, et al. The psychedelic future of post-traumatic stress disorder treatment. Curr Neuropharmacol. 2024;22:636–735.
42. Groen TV, Wyss JM. Connections of the retrosplenial granular a cortex in the rat. J Comp Neurol. 1990;300:593–606.
43. Groen TV, Wyss JM. Connections of the retrosplenial granular b cortex in the rat. J Comp Neurol. 2003;463:249–63.
44. Alexander AS, Nitz DA. Spatially periodic activation patterns of retrosplenial cortex encode route sub-spaces and distance traveled. Curr Biol. 2017;27:1551–1560.e4.
45. Yamawaki N, Corcoran KA, Guedea AL, Shepherd GMG, Radulovic J. Differential contributions of glutamatergic Hippocampal→Retrosplenial cortical projections to the formation and persistence of context memories. Cereb Cortex. 2019;29:2728–36.

46. Yamawaki N, Li X, Lambot L, Ren LY, Radulovic J, Shepherd GMG. Long-range inhibitory intersection of a retrosplenial thalamocortical circuit by apical tuft-targeting CA1 neurons. Nat Neurosci. 2019;22:618–26.
47. Miller AMP, Mau W, Smith DM. Retrosplenial cortical representations of space and future goal locations develop with learning. Curr Biol. 2019;29:2083–2090.e4.
48. Brennan EKW, Sudhakar SK, Jedrasiak-Cape I, John TT, Ahmed OJ. Hyperexcitable neurons enable precise and persistent information encoding in the superficial retrosplenial cortex. Cell Reports. 2020;30:1598–1612.e8.
49. Brennan EK, Jedrasiak-Cape I, Kailasa S, Rice SP, Sudhakar SK, Ahmed OJ. Thalamus and claustrum control parallel layer 1 circuits in retrosplenial cortex. Elife. 2021;10:e62207.
50. Alexander AS, Carstensen LC, Hinman JR, Raudies F, Chapman GW, Hasselmo ME. Egocentric boundary vector tuning of the retrosplenial cortex. Sci Adv. 2020;6:eaaz2322.
51. Whitesell JD, Liska A, Coletta L, Hirokawa KE, Bohn P, Williford A, et al. Regional, layer, and Cell-Type-Specific connectivity of the mouse default mode network. Neuron. 2021;109:545–559.e8.
52. Shepherd GMG, Yamawaki N. Untangling the cortico-thalamo-cortical loop: cellular pieces of a knotty circuit puzzle. Nat Rev Neurosci. 2021;22:389–406.
53. Jedrasiak-Cape I, Rybicki-Kler C, Brooks I, Ghosh M, Brennan EKW, Kailasa S, et al. Cell-type-specific cholinergic control of granular retrosplenial cortex with implications for angular velocity coding across brain states. Progress in Neurobiology, 251:102804.
54. Brooks IAW, Jedrasiak-Cape I, Rybicki-Kler C, Ekins TG, Ahmed OJ Unique transcriptomic cell types of the granular retrosplenial cortex are preserved across mice and rats despite dramatic changes in key marker genes. bioRxiv:2024.09.17.613545. 2024.
55. Alexander AS, Place R, Starrett MJ, Chrastil ER, Nitz DA. Rethinking retrosplenial cortex: perspectives and predictions. Neuron. 2023;111:150–75.
56. Valenstein E, Bowers D, Verfaellie M, Heilman KM, Day A, Watson RT. Retrosplenial amnesia. Brain. 1987;110:1631–46.
57. Nestor PJ, Fryer TD, Ikeda M, Hodges JR. Retrosplenial cortex (BA 29/30) hypometabolism in mild cognitive impairment (prodromal Alzheimer's disease). Eur J Neurosci. 2003;18:2663–7.
58. Tu S, Wong S, Hodges JR, Irish M, Piguet O, Hornberger M. Lost in spatial translation – A novel tool to objectively assess spatial disorientation in Alzheimer's disease and frontotemporal dementia. Cortex. 2015;67:83–94.
59. Walsh C, Ridler T, Margetts-Smith G, Garrido MG, Witton J, Randall AD, et al. β Bursting in the retrosplenial cortex is a neurophysiological correlate of environmental novelty which is disrupted in a mouse model of Alzheimer's disease. J Neurosci. 2022;42:7094–109.
60. Park K, Kohl MM, Kwag J. Memory encoding and retrieval by retrosplenial parvalbumin interneurons are impaired in Alzheimer's disease model mice. Curr Biol. 2024;34:434–443.e4.
61. Rolland Y, Andrieu S, Cantet C, Morley JE, Thomas D, Nourhashemi F, et al. Wandering behavior and Alzheimer disease. The REAL.FR Prospective Study. Alzheimer Dis Assoc Disord. 2007;21:31–38.
62. Vakulskas CA, Dever DP, Rettig GR, Turk R, Jacobi AM, Collingwood MA, et al. A high-fidelity Cas9 mutant delivered as a ribonucleoprotein complex enables efficient gene editing in human hematopoietic stem and progenitor cells. Nat Med. 2018;24:1216–24.
63. D'Amour JA, Ekins T, Ganatra S, Yuan X, McBain CJ. Aberrant sorting of hippocampal complex pyramidal cells in Type I Lissencephaly alters topological innervation. Elife. 2020;9:e55173.
64. Ekins TG, Mahadevan V, Zhang Y, D'Amour JA, Akgül G, Petros TJ, et al. Emergence of non-canonical parvalbumin-containing interneurons in hippocampus of a murine model of Type I lissencephaly. Elife. 2020;9:e62373.
65. Yao Z, van Velthoven CTJ, Kunst M, Zhang M, McMillen D, Lee C, et al. A high-resolution transcriptomic and spatial atlas of cell types in the whole mouse brain. Nature. 2023;624:317–32.
66. Yao Z, van Velthoven CTJ, Nguyen TN, Goldy J, Sedeno-Cortes AE, Baftizadeh F, et al. A taxonomy of transcriptomic cell types across the isocortex and hippocampal formation. Cell. 2021;184:3222–3241.e26.
67. Fantegrossi WE, Gray BW, Bailey JM, Smith DA, Hansen M, Kristensen JL. Hallucinogen-like effects of 2-([2-(4-cyano-2,5-dimethoxyphenyl) ethylamino] methyl)phenol (25CN-NBOH), a novel N-benzylphenethylamine with 100-fold selectivity for 5-HT2A receptors, in mice. Psychopharmacology. 2015;232:1039–47.
68. Buchborn T, Lyons T, Knöpfel T. Tolerance and tachyphylaxis to head twitches induced by the 5-HT2A agonist 25CN-NBOH in mice. Front Pharmacol. 2018;9:17.
69. Buchborn T, Lyons T, Song C, Feilding A, Knöpfel T. Cortical correlates of psychedelic-induced shaking behavior revealed by voltage imaging. Int J Mol Sci. 2023;24:9463.
70. Kim K, Che T, Panova O, DiBerto JF, Lyu J, Krumm BE, et al. Structure of a hallucinogen-activated Gq-coupled 5-HT2A serotonin receptor. Cell. 2020;182:1574–1588.e19.
71. Shibata H. Direct projections from the anterior thalamic nuclei to the retrohippocampal region in the rat. J Comp Neurol. 1993;337:431–45.
72. Shibata H. Efferent projections from the anterior thalamic nuclei to the cingulate cortex in the rat. J Comp Neurol. 1993;330:533–42.
73. Phillips JW, Schulmann A, Hara E, Winnubst J, Liu C, Valakh V, et al. A repeated molecular architecture across thalamic pathways. Nat Neurosci. 2019;22:1925–35.
74. Bécamel C, Berthoux C, Barre A, Marin P. Growing evidence for heterogeneous synaptic localization of 5-HT2A receptors. ACS Chem Neurosci. 2017;8:897–9.
75. Araneda R, Andrade R. 5-Hydroxytryptamine2 and 5-Hydroxytryptamine1a receptors mediate opposing responses on membrane excitability in rat association cortex. Neuroscience. 1991;40:399–412.
76. Tanaka E, North RA. Actions of 5-hydroxytryptamine of neurons of the rat cingulate cortex. J Physiol. 1993;69:1749–57.
77. Beique J-C, Imad M, Mladenovic L, Gingrich JA, Andrade R. Mechanism of the 5-HT2A receptor-mediated facilitation of synaptic activity in prefrontal cortex. PNAS. 2007;104:9870–5.
78. Newberry NR, Footitt DR, Papanastassiou V, Reynolds DJM. Actions of 5-HT on human neocortical neurones in vitro. Brain Res. 1999;833:93–100.
79. Chapin EM, Chapin EM, Andrade R. A 5-HT7 receptor-mediated depolarization in the anterodorsal thalamus. I. Pharmacological characterization. JPET. 2001;297:395–402.
80. Nardou R, Lewis EM, Rothhaas R, Xu R, Yang A, Boyden E, et al. Oxytocin-dependent reopening of a social reward learning critical period with MDMA. Nature. 2019;569:116–20.
81. Nardou R, Sawyer E, Song YJ, Wilkinson M, Padovan-Hernandez Y, de Deus JL, et al. Psychedelics reopen the social reward learning critical period. Nature. 2023;618:790–8.
82. Barre A, Berthoux C, Bundel DD, Valjent E, Bockaert J, Marin P, et al. Presynaptic serotonin 2A receptors modulate thalamocortical plasticity and associative learning. Proc National Acad Sci. 2016;113:E1382–E1391.
83. Berthoux C, Barre A, Bockaert J, Marin P, Bécamel C. Sustained activation of postsynaptic 5-HT2A receptors gates plasticity at prefrontal cortex synapses. Cereb Cortex. 2018;29:1659–69.
84. Carr DB, Cooper DC, Ulrich SL, Spruston N, Surmeier DJ. Serotonin receptor activation inhibits sodium current and dendritic excitability in prefrontal cortex via a protein kinase C-dependent mechanism. J Neurosci. 2002;22:6846–55.
85. Carr DB, Day M, Cantrell AR, Held J, Scheuer T, Catterall WA, et al. Transmitter modulation of slow, activity-dependent alterations in sodium channel availability endows neurons with a novel form of cellular plasticity. Neuron. 2003;39:793–806.
86. Lambe EK, Aghajanian GK. The role of Kv1.2-containing potassium channels in serotonin-induced glutamate release from thalamocortical terminals in ratfrontal cortex. Journal of Neuroscience. 2001;21:9955–63.
87. Marek GJ, Wright RA, Gewirtz JC, Schoepp DD. A major role for thalamocortical afferents in serotonergic hallucinogen receptor function in the rat neocortex. Neuroscience. 2001;105:379–92.
88. DeFelipe J, Fariñas I. The pyramidal neuron of the cerebral cortex: morphological and chemical characteristics of the synaptic inputs. Prog Neurobiol. 1992;39:563–607.
89. Voigts J, Harnett MT. Somatic and dendritic encoding of spatial variables in retrosplenial cortex differs during 2D navigation. Neuron. 2019;105:237–245.e4.
90. Keshavarzi S, Bracey EF, Faville RA, Campagner D, Tyson AL, Lenzi SC, et al. Multisensory coding of angular head velocity in the retrosplenial cortex. Neuron. 2022;110:532–543.e9. https://doi.org/10.1016/j.neuron.2021.10.031.
91. Poirier GL, Shires KL, Sugden D, Amin E, Thomas KL, Carter DA, et al. Anterior thalamic lesions produce chronic and profuse transcriptional deregulation in retrosplenial cortex: a model of retrosplenial hypoactivity and covert pathology. Thalamus Relat Syst. 2008;4:59–77.
92. Garden DLF, Massey PV, Caruana DA, Johnson B, Warburton EC, Aggleton JP, et al. Anterior thalamic lesions stop synaptic plasticity in retrosplenial cortex slices: expanding the pathology of diencephalic amnesia. Brain. 2009;132:1847–57.
93. Aggleton JP, O'Mara SM. The anterior thalamic nuclei: core components of a tripartite episodic memory system. Nat Rev Neurosci. 2022;23:505–16.
94. Sheeran WM, Ahmed OJ. The neural circuitry supporting successful spatial navigation despite variable movement speeds. Neurosci Biobehav Rev. 2020;108:821–33.
95. Vann SD, Aggleton JP, Maguire EA. What does the retrosplenial cortex do? Nat Rev Neurosci. 2009;10:792–802.
96. Rogers SA, Heller EA, Corder G Psilocybin-enhanced fear extinction linked to bidirectional modulation of cortical ensembles. bioRxiv:2024.02.04.578811. 2024. https://doi.org/10.1101/2024.02.04.578811.
97. Roy DS, Zhang Y, Aida T, Shen C, Skaggs KM, Hou Y, et al. Anterior thalamic circuits crucial for working memory. Proc Natl Acad Sci. 2022;119:e2118712119.
98. Ivan VE, Tomàs-Cuesta DP, Esteves IM, Luczak A, Mohajerani M, McNaughton BL, et al. Psilocybin reduces functional correlation and the encoding of spatial information by neurons in mouse retrosplenial cortex. Eur J Neurosci. 2024;60:6395–407.

ACKNOWLEDGEMENTS

This work was supported by: NIH R01MH129282; NIH R34NS127101; NIH P50NS123067; Alzheimer's Association Grant AARG-NTF-21-846572; NIH T32-DC000011; NIH T32-DA007268; NIH T32-NS076401; University of Michigan Eisenberg Family Depression Center Eisenberg Scholar Award.

AUTHOR CONTRIBUTIONS

Conceptualization: TGE, CRK, OJA; Investigation: TGE, CRK, TD, IAWB, IJC, ED, OJA. Formal Analysis: TGE, CRK, TD, IAWB, IJC; Visualization: TGE, CRK, TD, IAWB, IJC, OJA; Writing – Original Draft: TGE, CRK, OJA; Writing – Review & Editing: TGE, CRK, TD, IAWB, IJC, ED, OJA; Funding Acquisition & Supervision: OJA.

COMPETING INTERESTS

The authors declare no competing financial interest.

ETHICS APPROVAL

All methods in this study were performed in accordance with relevant guidelines and regulations. Animal procedures were carried out in accordance with these regulations and were approved by the University of Michigan Institutional Animal Care and Use Committees (IACUC), Protocol #11022.

ADDITIONAL INFORMATION

Supplementary information The online version contains supplementary material available at https://doi.org/10.1038/s41380-025-03257-w.

Correspondence and requests for materials should be addressed to Omar J. Ahmed.

Reprints and permission information is available at http://www.nature.com/reprints

Publisher's note Springer Nature remains neutral with regard to jurisdictional claims in published maps and institutional affiliations.

Open Access This article is licensed under a Creative Commons Attribution 4.0 International License, which permits use, sharing, adaptation, distribution and reproduction in any medium or format, as long as you give appropriate credit to the original author(s) and the source, provide a link to the Creative Commons licence, and indicate if changes were made. The images or other third party material in this article are included in the article's Creative Commons licence, unless indicated otherwise in a credit line to the material. If material is not included in the article's Creative Commons licence and your intended use is not permitted by statutory regulation or exceeds the permitted use, you will need to obtain permission directly from the copyright holder. To view a copy of this licence, visit http://creativecommons.org/licenses/by/4.0/.

© The Author(s) 2025